JOURNAL OF GEOPHYSICAL RESEARCH, VOL. 104, NO. B12, PAGES 28,859–28,878, DECEMBER 10, 1999

Effects of normal stress vibrations on frictional healing

Eliza Richardson and Chris Marone
Department of Earth, Atmospheric, and Planetary Sciences, Massachusetts Institute of Technology, Cambridge

Abstract. We conducted laboratory experiments to study frictional healing and the effects of normal stress vibrations on healing. The experiments were carried out using a servo-controlled double-direct shear apparatus on 10 cm x 10 cm blocks separated by a 3 mm-thick gouge layer of fine-grained (grain size of 75-212 μm) quartz powder. We performed slide-hold-slide tests in which sliding surfaces were driven at a constant velocity, halted for a given interval, then restarted at the prior driving velocity. Healing varied systematically with cumulative displacement, and by conducting several sets of identical slide-hold-slides we calibrated and removed these effects. Forward modeling of the healing and relaxation curves using the rate- and state-dependent friction laws shows that a displacement-dependent increase in the parameter b can account for our observations. To study the effects of vibration, we varied the mean normal stress of 25 MPa during holds by double amplitudes ranging from 1 to 13 MPa at a frequency of 1 Hz. Vibrations increased rates and magnitudes of frictional relaxation and healing, most likely due to increased gouge compaction. These effects increased with increasing amplitude of vibration. We performed normal stress step tests and used the results to model the vibrational slide-hold-slide tests. Rate- and state-dependent constitutive laws cannot adequately describe the behavior we observed experimentally because they neglect gouge compaction. Mechanisms such as normal force oscillations may explain faster fault healing rates than would be predicted by standard laboratory measurements at constant stress.

1. Introduction

Time-dependent frictional healing between slip events is a crucial part of the seismic cycle and is observable in both laboratory experiments [*Dieterich*, 1972, 1979; *Johnson*, 1981] and natural faults [*Vidale et al.*, 1994; *Marone et al.*, 1995]. Static and dynamic stress changes due to nearby earthquakes have been observed to affect fault healing and stability [*Mavko et al.*, 1985; *Spudich et al.*, 1995; *Wang and Cai*, 1997] or to trigger other earthquakes [*Hill et al.*, 1993; *Gomberg et al.*, 1997]. These effects have largely been interpreted and modeled only in the case of changes in shear stress resolved on to the fault [*Rice and Gu*, 1983; *Dieterich*, 1988], although often the accompanying change in normal stress is significant as well [*Mavko et al.*, 1985; *Linker and Dieterich*, 1992]. In addition, most laboratory rock friction experiments are conducted at constant normal stresses, thus preventing direct comparison of laboratory data with models and observations of the effect of stress changes during frictional healing.

Paper number 1999JB900320.
0148-0227/99/1999JB900320$09.00

Previous laboratory studies in rock friction have characterized the effects of changes in normal stress on steady state friction [*Linker and Dieterich*, 1992; *Dieterich and Linker*, 1992; *Wang and Scholz*, 1994]. These experiments have determined that a sudden change in normal stress produces a direct response in the direction of the normal stress change followed by a relaxation and subsequent evolution to a new steady state in friction. This process is analogous to the effect on friction of a sudden change in load point velocity. *Linker and Dieterich* [1992] have interpreted these results in the framework of the rate- and state-variable friction laws, while *Wang and Scholz* [1994] explained them in terms of a micromechanical contact model.

Studies of vibrated granular material [*Kudrolli et al.*, 1997; *Delour et al.*, 1999] have focused on establishing the fundamental behavior of particles subjected to vibrations. This includes particle velocities, trajectories, and collision energies. These experiments have typically been conducted at low normal stresses (< 1 MPa), at high velocities (10^0-10^3 mm/s), and with very high frequency stress oscillations (10^2-10^4 Hz). Nevertheless, their results are interesting in a geophysical context because understanding the dynamic properties of vibrated granular materials can lead to a better understanding of

how stress variations such as vibrations lead to changes in frictional parameters.

Effects of stress oscillations during steady sliding have been studied experimentally for metallic friction by *Broniec and Lenkiewicz* [1982]; *Skåre and Ståhl* [1992]; *Polycarpou and Soom* [1995a, b]. Since these investigators have been concerned primarily with the mechanical stability and wear experienced by moving machine parts, their experiments have also been conducted at low normal stresses, high velocities, and high frequencies compared to values that we expect to be relevant in tectonic environments. The experimental results have been somewhat inconsistent. All found that friction decreases in response to any vibrations in the direction of shearing. However, normal force vibrations are observed to cause either increases or decreases in friction. The former has been explained as contact welding or hardening between the metallic surfaces [*Broniec and Lenkiewicz*, 1982; *Skåre and Ståhl*, 1992], and the latter likely occurs when the amplitude of external vibrations is large enough to cause loss of contact between the surfaces or when their frequency is close to the resonant frequency of one of the contacting materials [*Broniec and Lenkiewicz*, 1982; *Hess and Soom*, 1991; *Tworzydlo and Becker*, 1991]. Additional observations from these experiments include the reduction of stick-slip behavior during vibration and the decrease in friction with increasing frequency of vibration [*Skåre and Ståhl*, 1992].

In this paper we report the impact of dynamic stressing on the rate and degree of frictional healing in laboratory friction experiments. We found that normal stress oscillations during quasi-stationary contact enhanced both frictional healing and relaxation and that this effect increased with increasing amplitude of oscillation.

2. Experimental Procedure

The experiments we describe were performed in a biaxial loading apparatus at room temperature, pressure, and humidity in the double-direct shear geometry (Figure 1 inset). The vertical ram driving the central block was controlled in displacement feedback, and the horizontal ram used to maintain normal stress was controlled in load feedback. The position and force of each ram are measured by displacement transducers (DCDTs) and load cells mounted on the rams. The shear load point position is measured at the end of the vertical ram where load is measured. The machine stiffness for the vertical load frame, which applies shear, is 5 MN/cm (250 MPa/cm for a 10 cm × 10 cm sample). Slip on the frictional surfaces and changes in gouge layer thickness were calculated using the calibrated apparatus stiffness from the load point and horizontal ram displacement, respectively. However, during dynamic variation in normal stress, we made direct measurements of gouge layer compaction using DCDTs mounted on the sample. Additional details of the experimental apparatus are given by C. Marone (manuscript in preparation).

Two 3-mm layers of fine-grained (91% of grains between 75 and 212 μm) silica powder (U.S. Silica F-110, 99.8% SiO_2) were sheared between either steel or Westerly granite samples. For the steel samples the side blocks measured 10 × 10 × 4 cm and the central block measured 10 × 15 × 4 cm. For the Westerly samples the side blocks measured 10 × 10 × 4 cm and the central block measured 10 × 15 × 8 cm. In this configuration the nominal area of frictional contact remains constant (10 cm × 10 cm) during sliding. The surfaces of the steel blocks contain horizontal grooves so that shear was forced to occur within the gouge layer. The surfaces of Westerly granite were surface ground flat to ±0.001 inch over their extent and then sand-blasted to increase roughness and inhibit boundary shear.

The normal force steps and vibrations were achieved by adding an external signal to the constant horizontal force maintained by servo-control (250 kN for all these experiments). A square wave with zero minimum or a trapezoidal wave with an instant increase but a ramp decrease was used for the normal stress steps. For the oscillations the added signal was a 1-Hz harmonic oscillation with zero mean. The amplitude of the steps and oscillations was controlled by adjusting the magnitude of the external signal and was set to zero during the parts of the experiments that were performed at constant normal stress (Table 1).

3. Data and Observations

We performed slide-hold-slide tests to measure frictional healing using the same method as outlined by *Dieterich* [1972] and *Beeler et al.* [1994]. In typical slide-hold-slide tests the load point is driven at a constant ve-

Table 1. Experimental Data

Experiment	Type	Amplitude, MPa
m081	displacement	0
m083	displacement	0
m085	displacement	0
m089	σ_n vibration	5.5[a]
m092	σ_n vibration	1.0[a]
m093	σ_n vibration	3.8[a]
m095	σ_n vibration	3.7[a]
m107	displacement	0
m113	σ_n vibration	5.6[a]
m114	σ_n vibration	11.5[a]
m117	σ_n vibration	5.6[a]
m134	σ_n vibration	12.5[a]
m223	σ_n vibration	3.7, 5.6[a]
m224	σ_n vibration	4.7, 2.8[a]
m225	σ_n vibration	10.4, 5.2[a]
m226	σ_n vibration	9.1, 8.0[a]
m237	σ_n step	0.2, 1.0[b]
m238	σ_n step	0.4, 1.2, 1.6, 2.2[b]
m272	σ_n step	1.2, 2.0, 2.5, 4.5[b]
m272	σ_n vibration	1.3, 1.9, 2.8, 3.8[a]

[a]Double amplitude.
[b]Single amplitude.

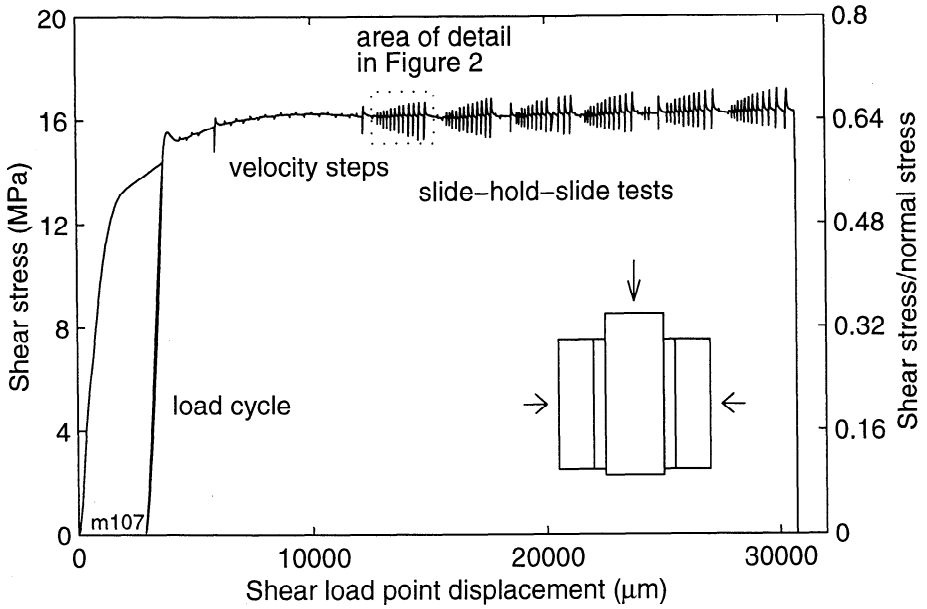

Figure 1. Shear stress versus shear displacement for a 3-mm gouge layer sheared at 10 μm/s between rough steel surfaces at 25 MPa normal stress. Shown are the initial loading, a load cycle, velocity steps, and six sets of slide-hold-slide tests. Detail of the first set of these is shown in Figure 2. Inset shows the double-direct shear configuration. The number in the bottom left corner refers to the experiment number in Table 1.

locity, halted for a given length of time, then restarted at the previous driving velocity. During the interval in which the load point is stationary, frictional strength relaxes as the shearing surfaces continue to creep. Upon reloading, the shearing surfaces restrengthen to some peak value of static friction, then evolve over some characteristic displacement, eventually returning to the same steady state value of sliding friction prior to the hold. We next present observations of frictional relaxation and healing that were used to characterize the effects of total displacement and variable normal stress on frictional restrengthening during quasi-stationary contact.

3.1. Effects of Displacement

In order to compare data from slide-hold-slide tests that included normal force vibrations to data from tests at constant stress, we first sought to eliminate other second-order effects that would also contribute to the rate and degree of frictional healing. Therefore we used a constant load point velocity, gouge layer thickness, and mean normal stress among all experiments. Within individual experiments, absolute displacement of the sliding surfaces also has an effect on frictional healing. To calibrate this effect, we performed several identical sets of slide-hold-slide tests over a range of absolute displacements (Figure 1).

This experiment was performed at a constant normal stress of 25 MPa. Before any shear load was placed on the sample, the normal load was set at 25 MPa, as with all the experiments. Then the vertical ram was started at a driving velocity of 10 μm/s. Next, a "load cycle" was performed in which the vertical ram was retracted at 10 μm/s until the shear load was removed completely, after which the ram was driven forward again, forming the hysteresis loop shown in Figure 1. Next, we executed a series of velocity step tests. During these tests, the load point velocity was rapidly increased from 10 to 20 μm/s. After a new steady state value of sliding friction was reached, the load point velocity was returned to 10 μm/s. This cycle was repeated continuously over the first 12 mm of displacement.

After $\sim$ 9 mm of shear displacement the system evolved from a strain-hardening regime to a velocity-weakening regime in which frictional resistance decreased with increasing slip speed. This transition has been noted by previous investigators and is thought to occur in response to the development of localized shear bands within the gouge layer [*Dieterich*, 1979; *Tullis and Weeks*, 1986; *Marone et al.*, 1990]. We waited until velocity weakening was reached before performing the slide-hold-slide tests.

The experiment shown in Figure 1 included six identical sets of slide-hold-slide tests. Each set was accomplished at a load point velocity of 10 μm/s and included two holds each for 3, 10, 30, 100, 300, and 1000 s (Figure 2). For each hold in each set we measured frictional healing ($\Delta\tau$) as the difference between steady state sliding shear stress just prior to stopping the load point and the peak value of shear stress reached upon reload. We measured frictional relaxation ($\Delta\tau_{\min}$) as the difference between steady state sliding shear stress and the minimum value of shear stress reached just before the load point was restarted. We also measured fault gouge com-

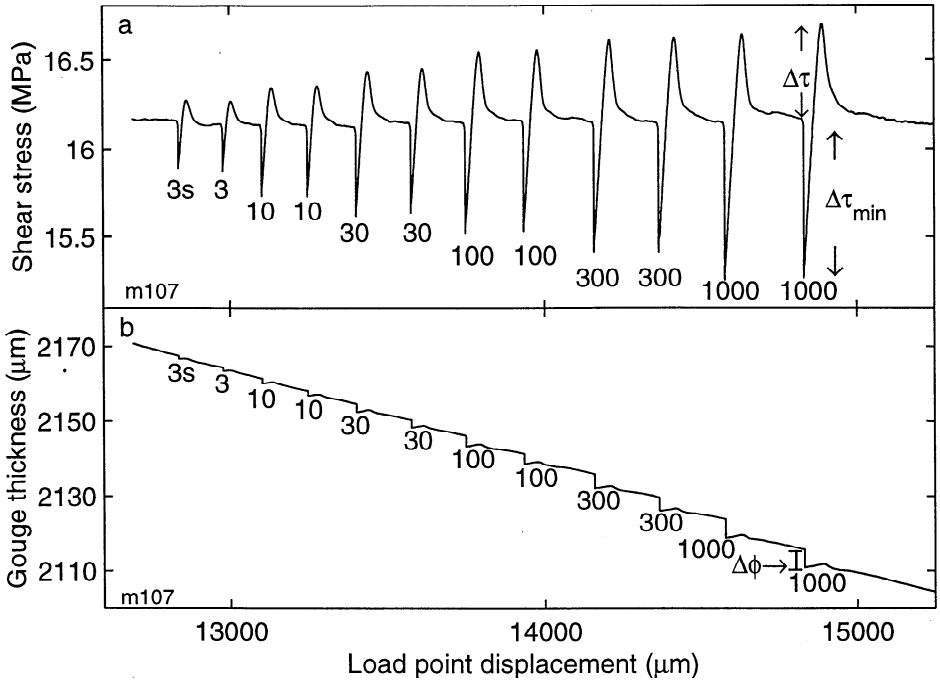

Figure 2. (a) Shear stress and (b) gouge layer thickness versus shear displacement for the first set of slide-hold-slide tests from Figure 1. Hold time in seconds is labeled beneath each hold. The measured quantities healing ($\Delta\tau$), relaxation ($\Delta\tau_{\min}$), and gouge compaction ($\Delta\phi$) are labeled on the last 1000-s hold. The continuous geometrical thinning of the gouge layer is inherent in the double-direct shear geometry [*Scott et al.*, 1994].

paction as the decrease in gouge layer thickness during the quasi-stationary hold (Figure 2b). We report values for healing and relaxation in terms of shear stress rather than friction to avoid confusion when we describe later experiments in which the normal stress was varied.

The magnitude of frictional healing, relaxation, and gouge compaction increases linearly with the logarithm of hold time (Figures 3a, 3b, and 3c). This result is in agreement with observations from previous studies that have measured frictional healing [*Dieterich*, 1972; *Johnson*, 1981; *Beeler et al.*, 1994] as well as relaxation and gouge compaction [*Marone*, 1998b; *Karner and Marone*, 1998]. In an individual experiment the magnitude of healing for equal hold times increases with displacement. In addition, the dependence of healing on log hold time increases with displacement. The dependence of the relaxation and compaction on displacement (Figures 3b and 3c) show just the opposite trend.

The 1000-s holds in each of the six sets of tests (Figures 3d, 3e, and 3f) show that healing, relaxation, and gouge compaction vary approximately logarithmically with increasing shear displacement. This effect of absolute displacement is also evident in the actual time series data (Figure 4) in which we compare two 100-s holds from the first and sixth tests at exactly the same scale.

We characterized the effects of displacement on the evolution of shear friction in order to eliminate them from our data. Once these effects were removed, we could determine the effects of other second-order variations, such as changes in normal stress.

3.2. Normal Stress Steps

We performed experiments similar to those described by *Linker and Dieterich* [1992] in which we rapidly stepped the normal force during steady sliding in order to observe the evolution of friction (Figure 5). For these experiments, sliding surfaces were driven at a constant speed of 10 μm/s, and the initial normal stress was 25 MPa. The magnitude of our normal stress steps ranged from 0.2 to 2.5 MPa, or 1-10% of the initial normal stress.

Like *Linker and Dieterich* [1992], we observed that shear stress increased instantly when the normal stress was stepped due to the Poisson effect. However, we found that the ratio of shear stress change to normal stress change was $\sim$ 0.01 for Westerly granite testing blocks and 0.02 for steel blocks. This is smaller by an order of magnitude than the ratio observed by *Linker and Dieterich* [1992]. This discrepancy is most likely due to the fact that they mounted their DCDTs directly on their sample blocks, and thus their effective stiffness was larger, and because their apparatus may have been slightly misaligned [*Linker and Dieterich*, 1992].

Following the Poisson effect, we observed elastic shear loading and subsequent evolution to steady state sliding at constant stresses. We measured the difference in

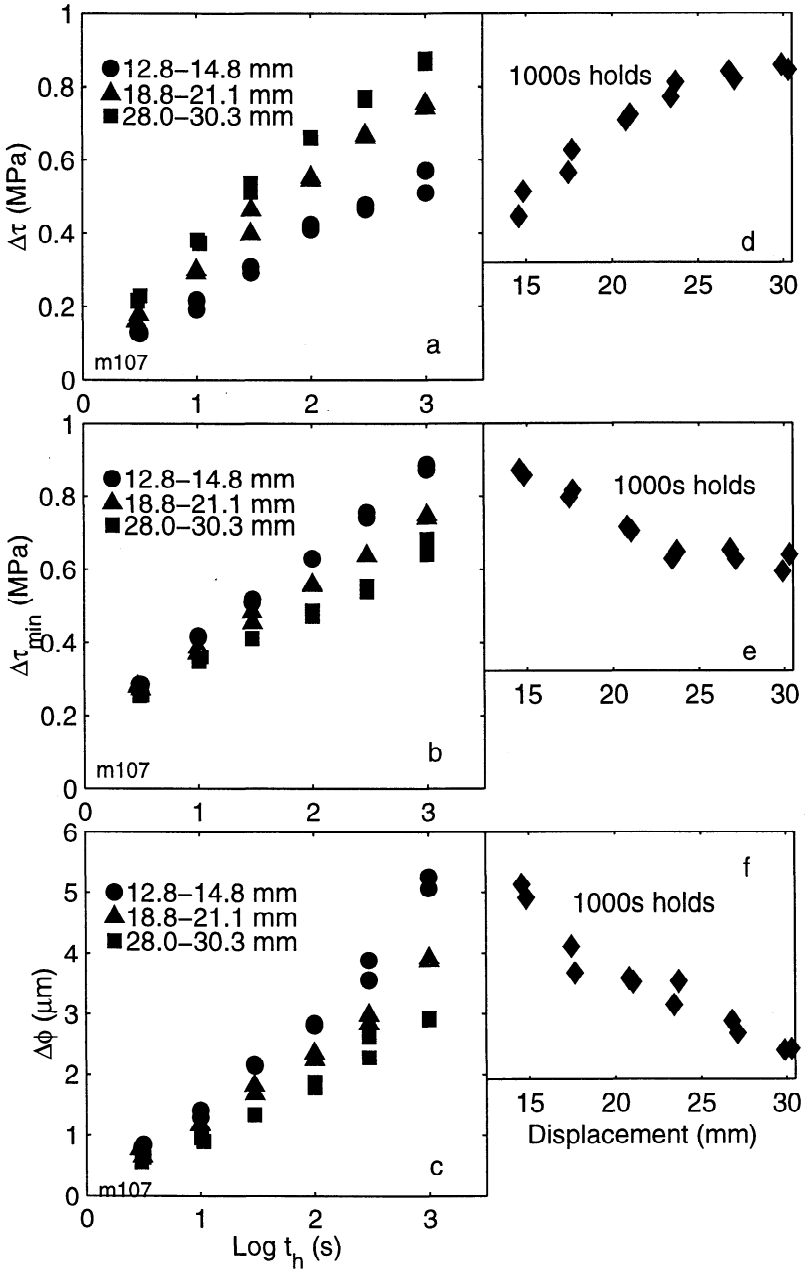

Figure 3. Time dependence of healing, relaxation, and compaction. For the first, third, and sixth sets of slide-hold-slide tests shown in Figure 1, (a) $\Delta\tau$, (b) $\Delta\tau_{min}$, and (c) $\Delta\phi$ are plotted versus $\log_{10}$ of hold time. Absolute shear displacement for each set is shown in the upper left. (d,e,f) Healing, relaxation, and compaction for each of the 1000-s holds in all six sets of slide-hold-slide tests as a function of absolute displacement.

shear stress between its value at the end of the elastic loading period and its subsequent steady state value in order to determine the quantity that *Linker and Dieterich* [1992] term "α," in which

$$\alpha = \frac{\Delta\tau_{\text{step}}/\sigma_{\text{final}}}{\ln(\sigma_{\text{final}}/\sigma_{\text{initial}})}. \quad (1)$$

Figure 6 shows one normal stress step. The point at which shear loading deviates from a linear elastic loading curve (τ_{elastic}) is marked with a circle. Note that the Poisson effect (marked with a diamond) is barely observable (Figure 6). It is clearly visible in the vibration tests with larger normal stress variations shown in later figures. The quantity $\Delta\tau_{\text{step}}$ is the difference between the steady state shear stress following the normal stress step and τ_{elastic} and is of interest because it is the evolution in shear stress that occurs with slip after the normal stress change. In order to determine the value of τ_{elastic} we incrementally fit a line to the shear loading curve, beginning with the data point corresponding to the beginning of the normal stress step. Each successive fit included one additional data point. We defined τ_{elastic} to be the data point corresponding to the last local minimum in the error of fit, thus the final data point

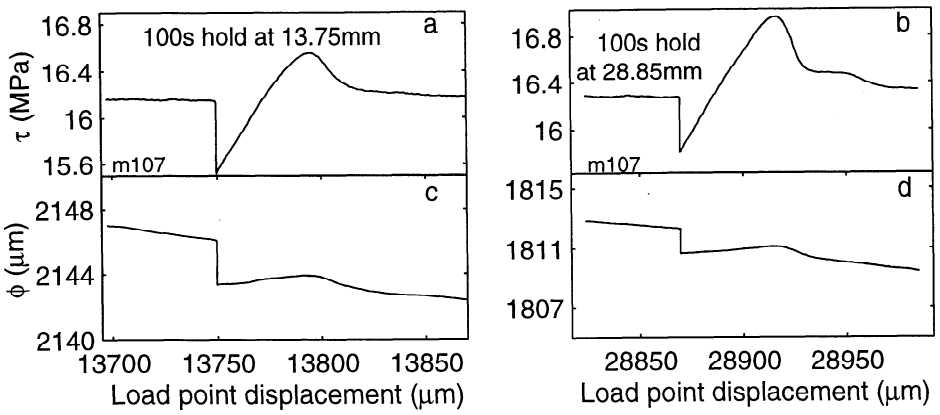

Figure 4. (a,b) Shear stress and (c,d) gouge layer thickness versus shear load point displacement for two 100-s slide-hold-slides at different displacements shown at the same scale. The slide-hold-slide on the left (Figures 4a and 4c) underwent greater relaxation and gouge compaction but less healing than the test at larger displacement (Figures 4b and 4d).

that belonged to the best fit line in a least squares sense.

Observations of the evolution of the gouge layer are as important as observations of shear stress in determining the effect of sudden normal stress steps on the frictional state of the system. We measured the changes in gouge layer thickness with two linear voltage differential transducers (LVDTs) mounted directly on the front face of the sample. The data we show (Figure 6c) are an average of the signal from these two sample-mounted LVDTs. As soon as the 2.5-MPa normal stress step was executed, the gouge layer compacted by about 5 μm. The gouge layer continued to compact rapidly during elastic loading. The point in displacement that marked the end of the elastic shear loading is marked on the gouge layer record with a circle (Figure 6c). The gouge layer continued to compact faster than at steady state over the same interval in displacement that corresponds to $\Delta\tau_{\text{step}}$, after which a new steady state was reached.

The slope (α) of the least-squares best fit line to measurements of $\Delta\tau_{\text{elastic}}/\sigma_{\text{final}}$ constrained to pass through the origin is 0.30 (Figure 7). *Linker and Dieterich* [1992] used an approximately similar method to determine τ_{elastic} and to find α; they obtained $\alpha = 0.2$. However, they also argue that α may be as large as 0.5; therefore our value seems reasonable. In sections 4.2-4.3, we use α to model data for normal stress steps and vibrational slide-hold-slide tests.

3.3. Normal Stress Vibrations

We tested the effects of normal stress oscillations on frictional healing by vibrating at a constant amplitude and frequency during the quasi-stationary inter-

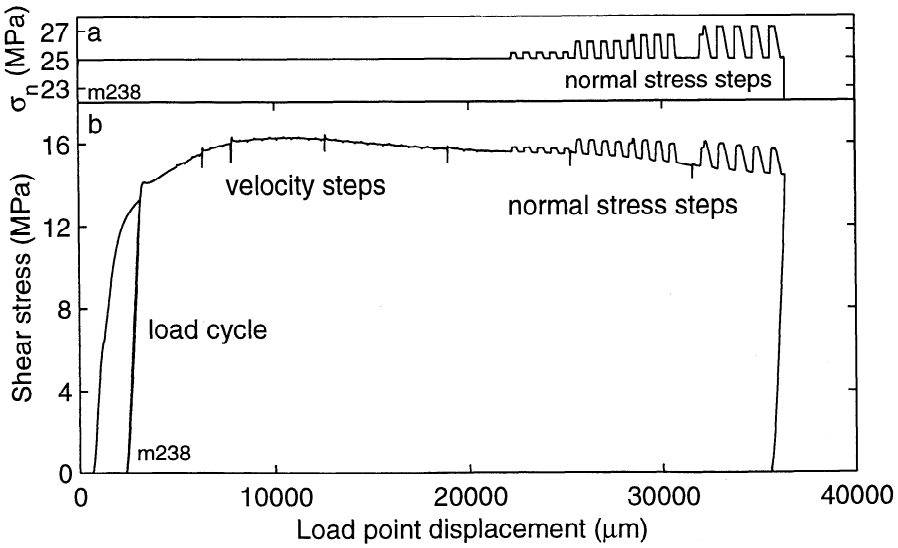

Figure 5. (a) Normal stress and (b) shear stress versus shear load point displacement for an experiment including four sets of normal stress steps (0.42, 1.20, 1.61, and 2.20 MPa). Normal stress was increased as rapidly as possible under servo control (each step occurred <0.2 s), but was ramped down to its initial value to prevent unstable sliding.

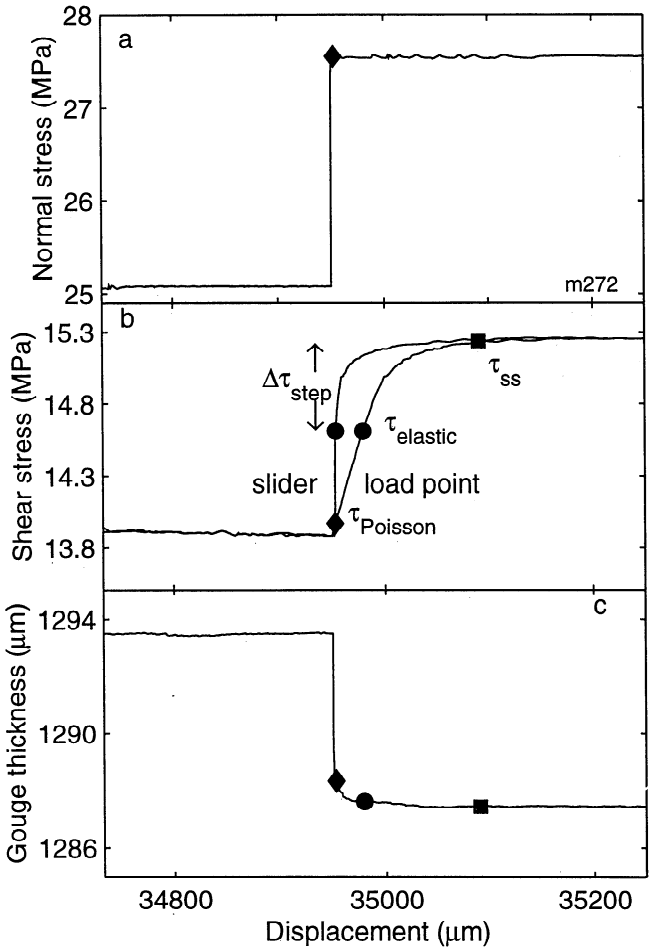

Figure 6. (a) Normal stress, (b) shear stress, and (c) gouge layer thickness as a function of shear displacement for one normal stress step. Normal stress and layer thickness are shown versus the load point displacement; shear stress is shown versus both load point displacement and slip measured directly across the sliding surfaces. The 2.5-MPa step in normal stress was accomplished in (<0.2 s). The shear stress increased instantaneously by 0.05 MPa due to Poisson expansion of the central forcing block (marked with a diamond). The shear stress followed an elastic loading curve until $\tau_{elastic}$ (marked with a circle), then evolved to a new steady state (marked with a square); the difference between the new steady state and $\tau_{elastic}$ is $\Delta\tau_{step}$. The displacements at which $\tau_{Poisson}$, $\tau_{elastic}$, and τ_{ss} occur are also marked on the layer thickness curve. The effects of continual geometric layer thinning have been removed.

vals of the slide-hold-slide tests. All of the experiments with normal stress oscillations were started exactly the same way as the experiment in Figure 1. Following the standard loadup and initial shearing procedure, slide-hold-slide tests with normal force oscillations were performed. These were usually followed by another set at constant stress or by another set of slide-hold-slides with oscillations (Figure 8).

Normal stress vibrations were accomplished by first stopping the vertical ram as in a standard slide-hold-slide, then ramping up the amplitude of the normal force oscillations to some constant amplitude ($2A = 5.6$ MPa for the experiment in Figure 8). These oscillations were maintained for a given time interval, then reduced to zero amplitude again before the vertical ram was restarted. Figure 9 shows this procedure in detail for one 30-s slide-hold-slide test with normal force oscillations of 4.7-MPa double amplitude.

There was a lag of a few seconds at the beginning (t_1 - t_2 in Figure 9) and end (t_5 - t_6) of every vibrational hold since the vibration amplitude was adjusted by hand. Similarly, there was a finite time over which the normal force oscillations were increased to the chosen amplitude (t_2 - t_3) and decreased back to zero (t_4 - t_5). We chose to increase/decrease the amplitude of the oscillations gradually in order to maintain constant frequency and so that the total signal to the servo-control varied smoothly at the onset and end of the vibrations. This prevented unstable sliding at the beginning of holds associated with large-amplitude reductions in normal stress. These short time lags were approximately constant for all holds because they only depended on the reflexes of the operator. The vibrational hold time was generally 5-7 s less than the total "hold time"; however, we always report the total hold time. This discrepancy necessarily affects short holds more than long ones, but we assume the effect is negligible and do not correct for it in any way.

3.3.1. Frictional healing The most significant effect of vibration during holds was the overall degree of frictional relaxation and subsequent restrengthening.

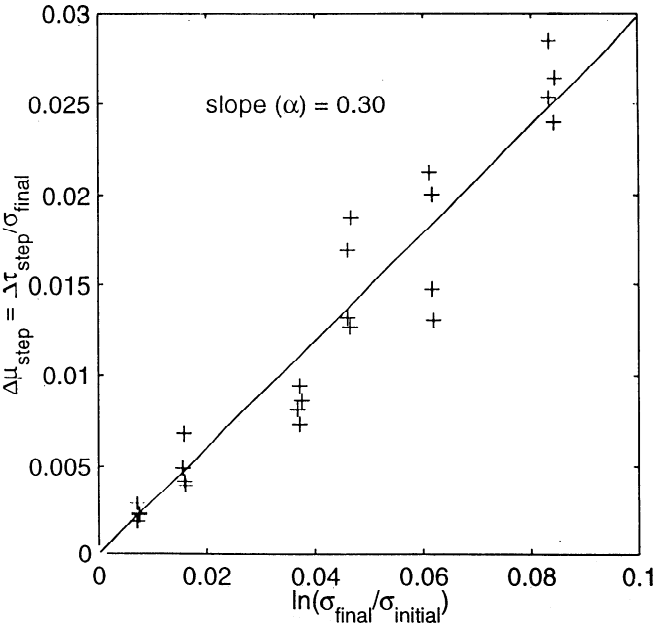

Figure 7. Nonelastic change in shear strength ($\Delta\tau_{step}$) upon a step change in normal stress (see Figure 6b). $\Delta\tau_{step}$ is normalized by final normal stress and plotted versus the natural logarithm of the ratio of the final to the initial normal stress for 24 normal stress step tests. The line is the least squares best fit line to the data constrained to pass through the origin. Its slope, 0.30, equals α [*Linker and Dieterich*, 1992].

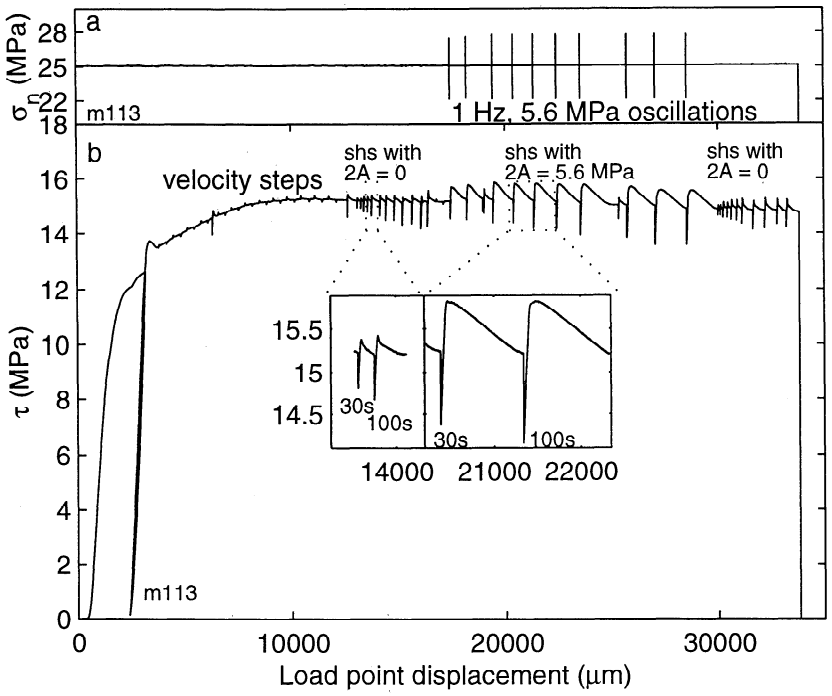

Figure 8. (a) Normal stress and (b) shear stress versus shear displacement for a 3-mm gouge layer sheared at 10 μm/s between sand-blasted Westerly granite surfaces. The first and third sets of slide-hold-slide tests were performed at constant normal stress (25 MPa). During the second set of slide-hold-slide tests, normal stress was oscillated at 1 Hz and a $2A = 5.6$ MPa for the duration of the hold, then returned to 25 MPa at the end of the hold. The Figure 8a inset figure shows four slide-hold-slides (right) with and (left) without vibrations.

The inset detail in Figure 8 compares two nonvibrational holds with two vibrational holds of equal times. These two pairs are shown at the same scale. Clearly, relaxation and especially healing, which more than doubled in comparison to the holds at constant stress, increased greatly during vibration. Notice that the peak level of friction upon reloading is not as clearly defined in the vibrational holds as in the constant stress holds. This rounded shape at peak friction was characteristic of vibrational holds. For the purpose of measuring frictional healing, we defined the peak friction as the greatest value attained after the hold, even if this value occurs at some displacement after an apparent local maximum in friction (e.g., the 100-s hold shown in Figure 8 inset).

Another typically observed consequence of normal force vibrations was the unusually large displacement over which sliding friction returned to its previous steady state value (Figure 8). This displacement is greater than that for longer constant normal stress holds that reached equivalent values of healing and peak friction. In addition, it is clear that frictional healing depends less strongly on hold time for vibrational holds than for holds at constant stress (compare slopes of the open and solid symbols in Figure 10b). This feature is common for vibrational holds and seems to be related to the amplitude of vibration. Specifically, increasing vibration amplitude decreases the healing rate, β, defined here as $\beta = \Delta\tau/\Delta \log t_h$ in which t_h is the hold time [*Marone*, 1998b]. In fact, for very large amplitude vibrations ($2A \approx$ 10-13 MPa), $\beta \approx 0$ for the range of hold times in these experiments; however, unstable sliding marked by sudden shear stress drops tended to occur during holds with large-amplitude vibrations, making these data and the related relaxation data somewhat difficult to interpret. In contrast to frictional healing and relaxation, gouge layer compaction consistently increased with hold time to a greater degree during vibrational holds than during constant stress holds (Figure 10).

Figure 10 compares healing ($\Delta\tau$), relaxation ($\Delta\tau_{\min}$), and gouge layer compaction ($\Delta\phi$) for holds with and without normal stress oscillations for the three sets of slide-hold-slide tests displayed in Figure 8. Figures 10a, 10b, and 10c show measurements made on raw data, and Figures 10d, 10e, and 10f show measurements that have been corrected for the effects of absolute displacement. The displacement correction was determined by fitting a logarithmic curve to data of healing (or relaxation or gouge compaction) as a function of displacement (Figure 3) taken from the displacement calibration experiments such as the one shown in Figure 1 and others (see Table 1). The difference in healing on the calibration curve between the actual displacement and some reference displacement was the value of the correction added to the data and was applied iden-

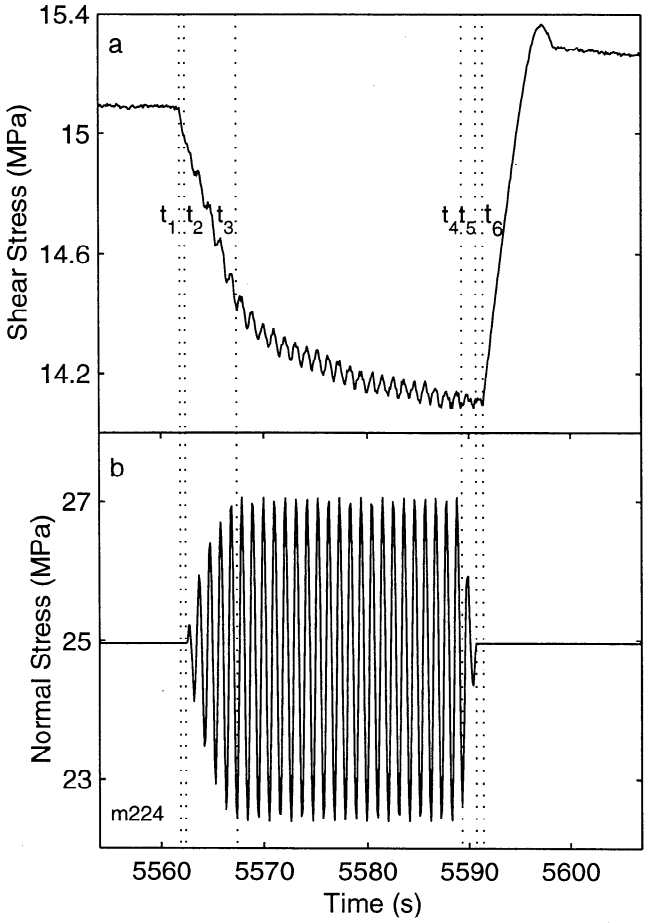

Figure 9. (a) Shear stress and (b) normal stress versus time for one 30-s hold with 4.7-MPa normal stress oscillations. The vertical ram was stopped at t_1. At t_2, the sinusoidal normal stress oscillations were started, reaching 5.6-MPa double amplitude at t_3. At t_4 the amplitude of the oscillations was decreased gradually, becoming zero at t_5. The vertical ram was restarted at t_6, ending the hold. The apparent 10-s modulation in amplitude of the normal stress during oscillations was due to a data-sampling rate of 10 Hz slightly out of phase with the 1-Hz oscillations. The oscillations in shear stress are due to direct elastic coupling (Poisson effect) between the normal and shear stress resolved on the central forcing block.

tically to all the vibration experiments detailed here. We assumed that since the initial shear loadup was the same in each experiment, the effects of displacement were nearly identical for all of our experiments for the ranges of displacements ($\approx$ 10-35 mm) at which we conducted the slide-hold-slide tests. In the plots on the right of Figure 10, all the data are shown at a reference displacement of 15 mm. We did not observe any permanent effects of vibration, as is evident from the good agreement between the data from first and third slide-hold-slide tests.

Frictional healing increases with the log of hold time for both constant stress and vibrational holds (Figures 10a and 10b). The absolute level of healing is much larger for vibrational holds. An extrapolation of a least squares best fit line to these data implies that a hold of $\sim 3 \times 10^5$s at constant normal stress will result in the same level of frictional healing as a 10 s hold with 5.6-MPa vibrations (Figure 10).

Frictional relaxation also increases with the logarithm of hold time for both types of holds (Figures 10c and 10d). Relaxation depends more strongly on hold time for vibrational holds (i.e., the slope of the best fit line is slightly steeper for the vibrational set), and the absolute level of relaxation is greater by approximately the same amount as that for healing (note the factor of 2 change in vertical scale between the healing and relaxation parts of Figure 10). This was observed consistently in all experiments. Gouge compaction greatly increased during normal force oscillations and also depends more strongly on hold time than it does under a constant normal load (Figures 10e and 10f). Inspection of the gouge layer after an experiment with large-amplitude vibrations revealed that the gouge had consolidated to form weakly cohesive plates of the order of centimeters in area and fractions of a millimeter in width due to the great compaction induced by the vibrations. Gouge layer effects are probably the most important for characterizing the effects of vibration as will be discussed.

3.3.2. Effects of vibration amplitude We conducted several slide-hold-slide tests using different vibration amplitudes (Figure 11). For equal hold times the total change in shear stress during the hold and reload, $\Delta\tau + \Delta\tau_{\min}$, (Figure 11d), and the gouge compaction during the hold (Figure 11e) both increase approximately linearly with vibration amplitude. The delayed return to steady state friction and the rounded peak in friction following a hold are also enhanced with increasing amplitude (Figures 11a, 11b, and 11c). We measure total change in shear stress ($\Delta\tau + \Delta\tau_{\min}$) in Figure 11d because 75% of holds with double amplitudes of 6 MPa and greater experienced unstable sliding at the onset of vibrations, creating a small but unrecoverable shear stress drop (e.g., Figure 12). These stress drops could sometimes be eliminated by a longer ramp in vibration amplitude or a longer lag at the beginning of the hold before starting the vibrations.

3.3.3. Gouge layer effects We measured the degree of gouge layer compaction as the change in layer thickness during the hold (Figures 2b and 13a) and dilatation as the change in gouge layer thickness between the end of the hold and the new steady state reached after the end of the hold (Figure 13a). We have already noted that healing, relaxation, and compaction vary linearly with the logarithm of hold time (Figures 3 and 10) and that gouge compaction and the total change in shear stress both vary approximately linearly with the amplitude of vibration for a given hold time (Figure 11). Thus the relationship between changes in shear stress and changes in the gouge layer during slide-

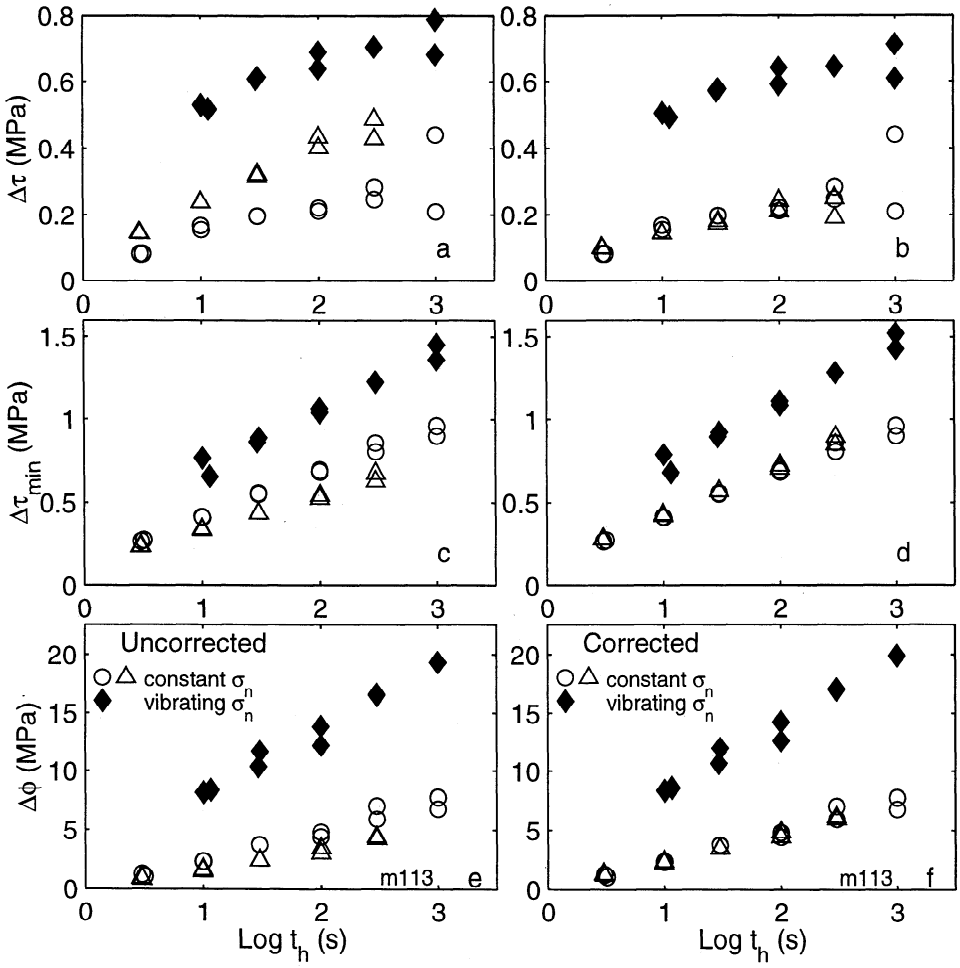

Figure 10. (a,b) Measurements of $\Delta\tau$, (c,d) $\Delta\tau_{\min}$, and (e,f) $\Delta\phi$ plotted versus $\log_{10}$ of hold time for the three sets of slide-hold-slide tests in Figure 8. Effects of absolute displacement have been accounted for in the data on the right (Figures 10b, 10d, and 10f). Open circles and triangles represent the data from the first and third sets of slide-hold-slide tests, respectively, that were performed at constant normal stress. Solid diamonds represent the data from the second set with oscillating normal stress ($2A = 5.6$ MPa).

hold-slide tests may be important in characterizing the effects of vibration.

In fact, we found that total change in shear stress varies linearly with both compaction and dilatation (Figures 13b and 13c) over a range of vibration amplitudes. In the experiment shown in Figures 13b and 13c, hold times ranged from 3 to 1000 s. As hold time increases, compaction and total change in shear stress increase, so even though time is not explicitly plotted, the hold time increases from left to right within each of the three data sets. Note that a 1000-s hold with no vibrations underwent approximately the same amount of compaction as a 12-s hold with 8.0-MPa vibrations. Likewise, shorter hold times with 9.1-MPa vibrations achieved greater compaction and thus greater healing and relaxation than longer hold times with 8.0-MPa vibrations. This suggests that the effect of vibrations during a hold is essentially to trade time for compaction. Most dilatation measurements approached the minimum resolution of our LVDTs, so there is more scatter in this data set. However, it is still evident that there is a similar trade-off between time and dilatation when the gouge layer undergoes vibration. We will later discuss how the changing state of the gouge layer can be important in modeling the effects of normal force vibrations during slide-hold-slide tests.

4. Discussion

We have modeled the experiments to determine if the dependence of frictional healing on second-order effects such as cumulative slip and variable normal stress are consistent with the existing framework of the rate and state friction laws. Although other theoretical interpretations are possible and plausible, we are only considering the rate and state empirical friction laws here.

In the case of the constant stress holds, we adopted the standard law

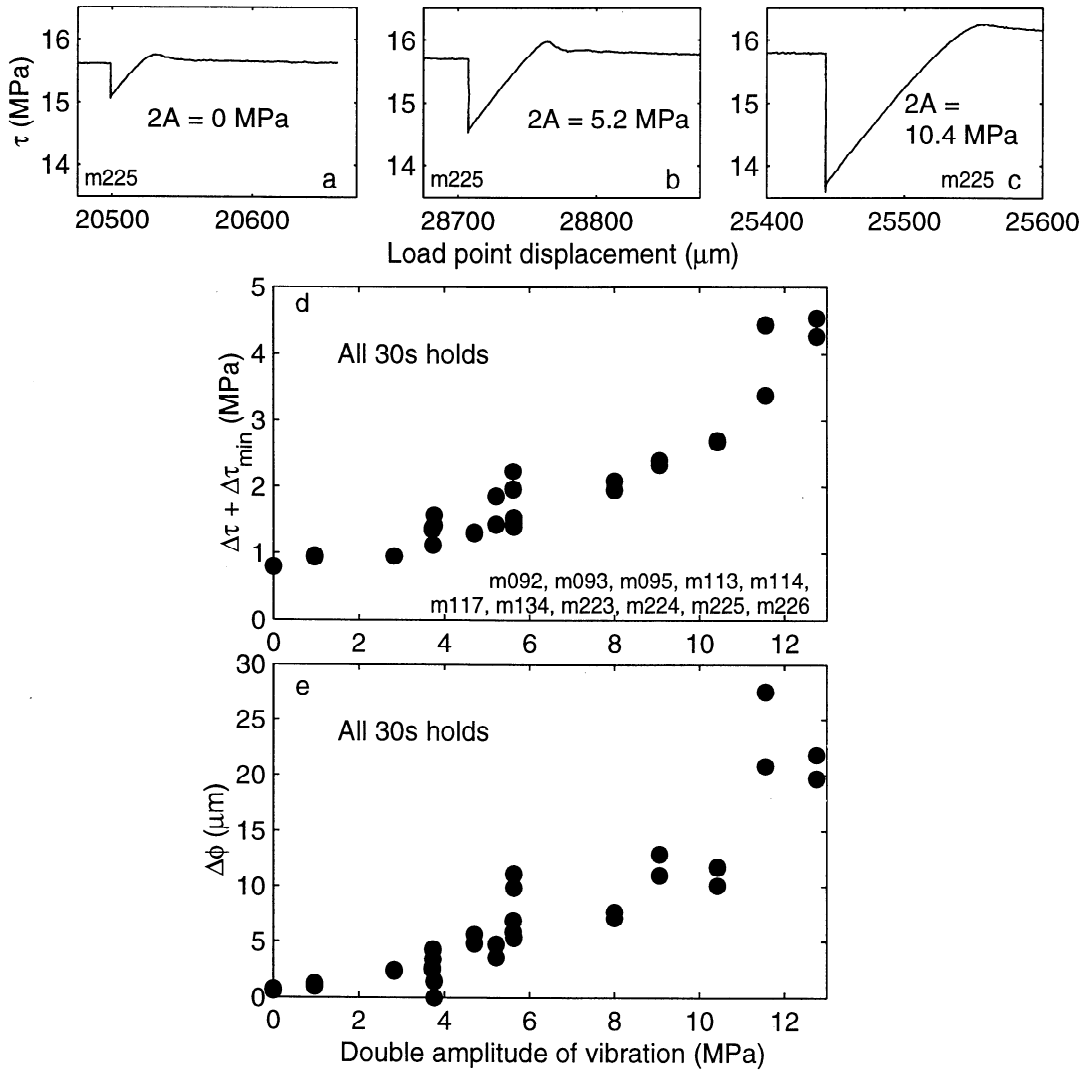

Figure 11. Shear stress versus shear load point displacement for 30-s holds from one experiment at (a) constant normal stress, (b) $2A = 5.2$ MPa, and (c) $2A = 10.4$ MPa. Total shear stress change ($\Delta\tau + \Delta\tau_{min}$) versus (d) $2A$ and (e) $\Delta\phi$ are presented at a reference displacement of 30 mm.

$$\mu = \mu_0 + a \ln\left(\frac{V}{V_0}\right) + b \ln\left(\frac{V_0\theta}{D_c}\right) \tag{2}$$

in which μ_0 is the coefficient of friction at the steady state sliding velocity V_0, V is the slip rate, θ is the state variable that can represent average contact lifetime, D_c is the characteristic slip distance over which friction evolves to a new steady state following a change in velocity, and a and b are empirical constants. Equation (2) was coupled to a single-degree-of-freedom elastic relationship,

$$\frac{d\mu}{dt} = k(V_{lp} - V) \tag{3}$$

in which k is the apparatus stiffness divided by the normal stress ($1 \times 10^{-3}\mu\text{m}^{-1}$ for our apparatus) and V_{lp} is the slip rate of the load point, which is set equal to V_0. We tested two evolution laws with our data. One, the Dieterich, or "slowness" law, is given by

$$\frac{d\theta}{dt} = 1 - \frac{V\theta}{D_c} \tag{4}$$

in which θ evolves with time [*Dieterich*, 1978, 1979]. The other, the Ruina, or "slip" law, is given by

$$\frac{d\theta}{dt} = \frac{-V\theta}{D_c} \ln\left(\frac{V\theta}{D_c}\right) \tag{5}$$

in which θ evolves with slip [*Ruina*, 1983].

In the case of the normal stress steps and the slide-hold-slide tests with normal stress oscillations, we followed the formulation of *Linker and Dieterich* [1992] in which a change in normal stress causes an immediate change in the state variable of the form

$$\theta = \theta_0 \left(\frac{\sigma_{\text{initial}}}{\sigma_{\text{final}}}\right)^{\alpha/b}, \tag{6}$$

where α is defined in (1). After this sudden decrease

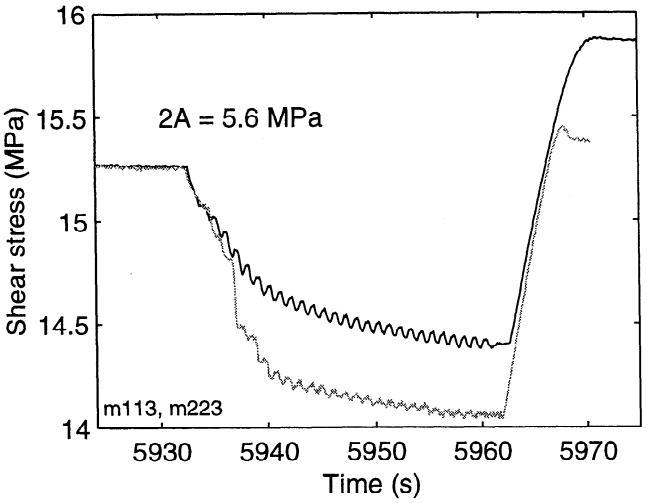

Figure 12. Shear stress versus time for two 30-s hold times with the same double amplitude of σ_n vibrations from different experiments. One has a small stress drop (shaded), and the other does not (solid). At the end of the hold, relaxation and healing differ between the two by an amount approximately equal to that of the stress drop.

in state, θ evolves according to either (4) or (5) [*Linker and Dieterich*, 1992].

4.1. Displacement

In the case of total displacement, other workers have noticed changes in friction parameters with increased accumulated slip [*Dieterich*, 1981; *Lockner et al.*, 1986; *Beeler et al.*, 1996]. Such effects are generally considered to be a transient phase that occurs at low total displacements after which friction parameters become independent of accumulated slip if the wear rate is low and gouge particle size distribution does not continue to evolve. Previous work in characterizing the effect of displacement on frictional behavior has generally concentrated on slip stability, the friction rate parameter, and gouge layer thickness and roughness [*Marone*, 1998a]. For example, it has been established that thick gouge layers tend to stabilize slip at small displacements [*Marone et al.*, 1990]. As displacement accumulates, the friction rate parameter decreases for gouge layers and becomes velocity weakening [*Dieterich*, 1981; *Beeler et al.*, 1996]. We also observe this transition at $\sim$ 7-10 mm of total displacement. Further detailed discussion of displacement effects has been given by *Marone* [1998a] and is not repeated here.

Our observations suggest that for thick gouge layers, shear localization evolves further over the course of an experiment, as discussed by *Marone and Kilgore* [1993], an important consideration when comparing data from different parts of an experiment. The conclusion that gouge evolution continues after the transition to velocity weakening is also supported by the results of *Beeler et al.* [1996], who found that gouge returns to a velocity-strengthening regime in their rotary shear experiments after very large displacements (>100 mm).

We simulated the healing and relaxation data by solving (2) and (3) numerically with either the Dieterich or Ruina evolution law. We used values of a, b, and D_c taken from inversions of velocity steps from the same experiments. The Dieterich law fits both the healing and relaxation data sets from the first set of tests in the experiment shown in Figure 1 (solid circles in Figures 14a and 14c) acceptably with $a = 0.008$, $b = 0.005$, and $D_c = 15\mu$m (solid lines in Figures 14a and 14c). The Ruina law fit to the same data had $a = 0.008$, $b = 0.007$, and $D_c = 15\mu$m (solid lines in Figure 14b and 14d). In order to fit the healing and relaxation measurements

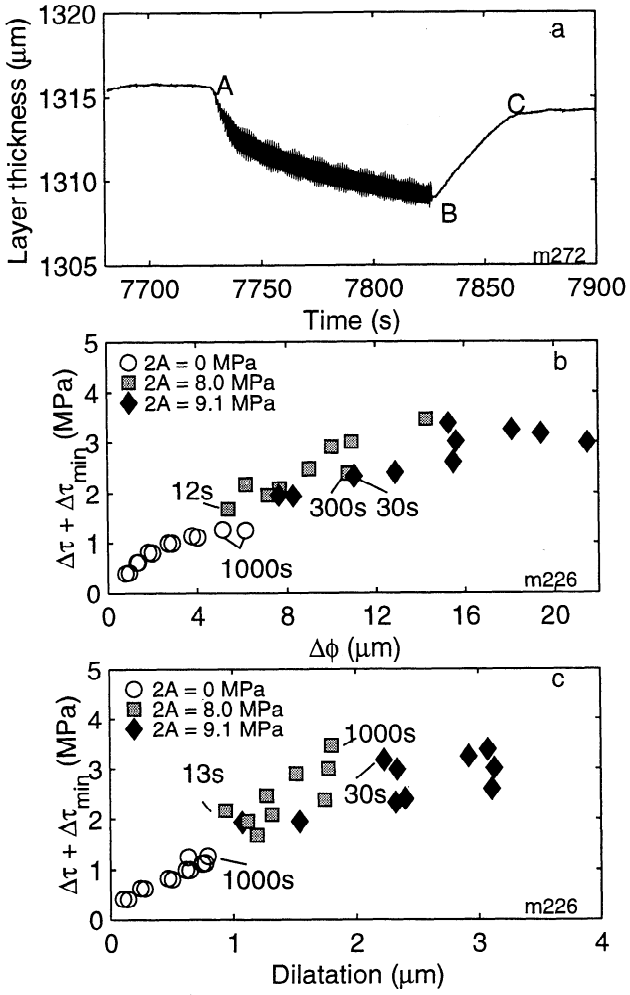

Figure 13. Layer thickness (a) versus time for one slide-hold-slide test and measurements of $\Delta\tau + \Delta\tau_{min}$ as a function of (b) compaction and (c) dilatation (c) for several hold times. The data shown in (Figure 13a) are from an LVDT mounted directly on the sample, and geometric thinning has been removed. Compaction is the difference between A and B and dilatation is the difference between C and B. Open circles show slide-hold-slide tests without vibrations ($3 \leq t_h \leq 1000$ s), shaded squares show tests with $2A = 8$ MPa ($12 \leq t_h \leq 1000$ s), and solid diamonds show slide-hold-slide tests with $2A = 9.1$ MPa ($11 \leq t_h \leq 1000$ s).

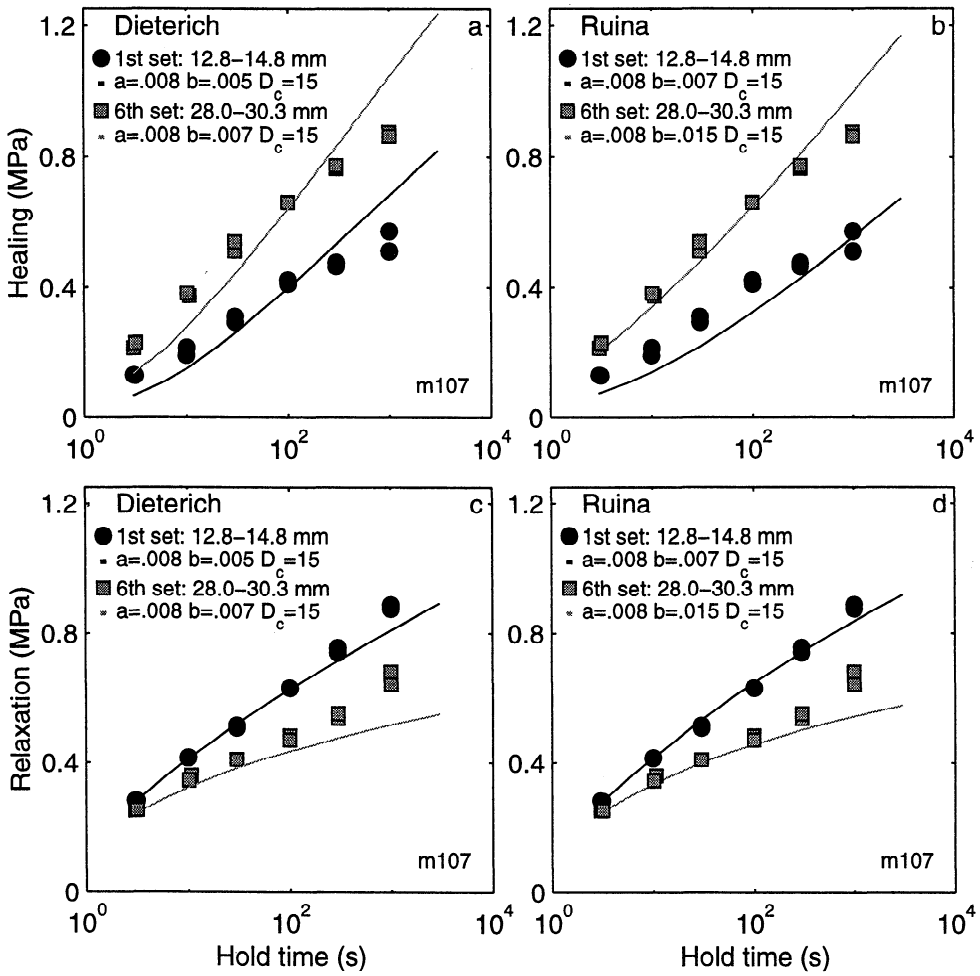

Figure 14. Data (symbols) and simulations (lines) obtained from forward modeling the first and sixth set of (a,b) healing and (c,d) relaxation measurements from the experiment in Figure 1. Circles and solid lines represent data and simulations from the first set, squares and shaded lines represent data and simulations from the sixth set of slide-hold-slide tests. The left and right sets of plots show the same data, but the models on the left (Figures 14a and 14c) use the Dieterich evolution law while the models on the right (Figures 14b and 14d) use the Ruina law. These plots show results of four, not eight, simulations: one each for each data set using each law. For instance, the healing and relaxation data for the first set of slide-hold-slide tests in Figures 14a and 14c are both fit simultaneously by the same Dieterich model.

from the sixth set of slide hold slide tests in the same experiment (Figure 14, shaded squares), we increased b to 0.007 in the Dieterich law and to 0.015 in the Ruina law but kept other parameters the same. The increase in b simultaneously reproduced the increased rate of frictional healing and the reduced degree of frictional relaxation (Figure 14, shaded lines). In general, we were able to simulate the slip dependence of frictional healing entirely with an increase in b.

We also compared the forward model to the time series data (Figure 15). The forward model used the same values of a, b, and D_c as the fit to healing data (Figure 14); thus there are no free parameters in the comparison of Figure 15. These fits are reasonable and show that the change in frictional healing and relaxation that we observe as a function of cumulative slip can be accounted for entirely by an increase in b. An increase in the parameter b was found to occur along with a decrease in gouge layer thickness in the triaxial experiments of *Marone et al.* [1990]. This may be relevant to what we observe. Probably, the gradual compaction of the gouge layer and localization of shear bands is the cause of the change in healing and relaxation that we observe with displacement.

This displacement effect is significant well after the transition to velocity weakening or steady state sliding friction, both of which usually occurred in our experiments between 7 and 10 mm of total slip. It is important to take this effect into account, especially when comparing data from the same experiment in which the effects of other second-order effects are being tested, such as variable normal stress or driving velocity.

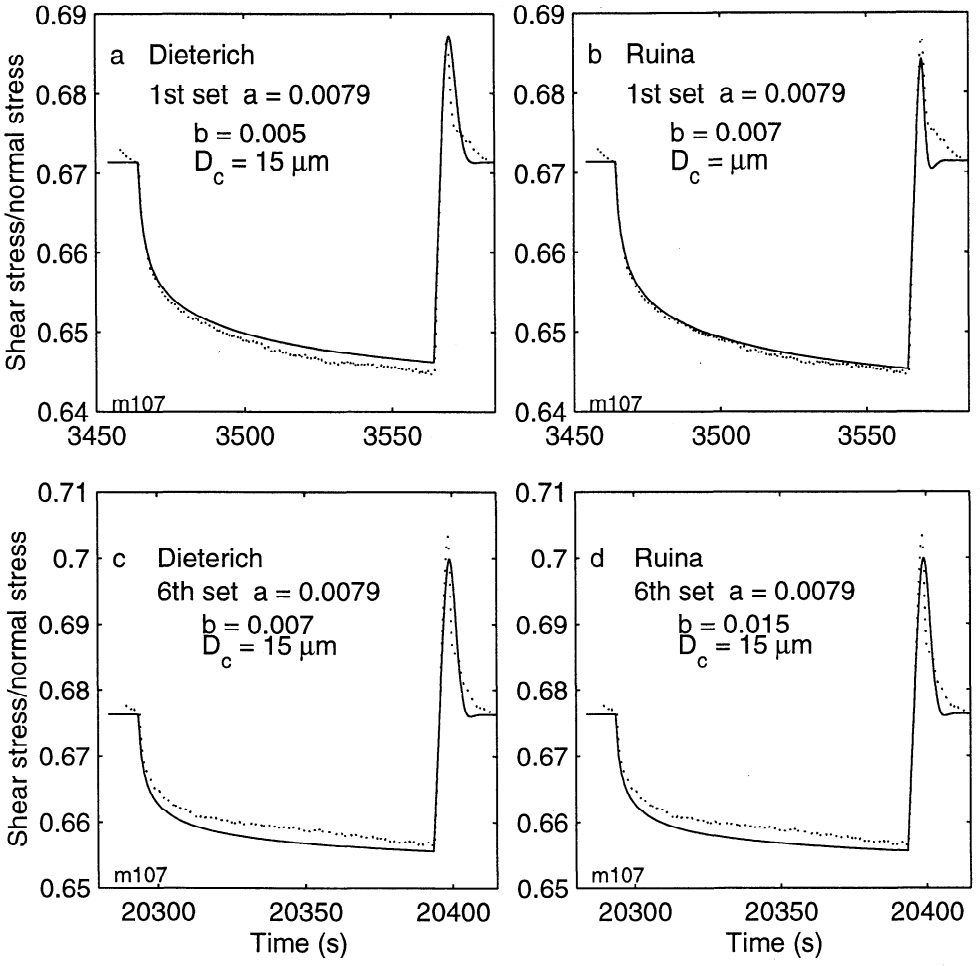

Figure 15. Fit to two 100-s slide-hold-slide tests from the (a,b) first and (c,d) sixth sets of holds in the experiment from Figure 1. Both sets of plots show the same data (dotted lines), but the plots on the left (Figures 15a and 15c) show models using the Dieterich law and the plots on the right (Figures 15b and 15d) show models using the Ruina law (solid lines). We used the same parameters in these forward models as in Figure 14. These fits are good considering that there were no free parameters.

4.2. Normal Stress Steps

The key difference in describing the evolution of the state variable after a change in normal stress as opposed to a change in driving velocity is that upon stepping the normal stress, state immediately decreases, as described by (6). Micromechanically, this situation can be thought of as a decrease in the average lifetime of contacts in the system, since new ones have been created by the sudden compaction of the granular layer induced by the increase in normal stress. In addition, if the instantaneous growth of preexisting contacts is considered not as an increase in the lifetime of the old contacts but, rather, as new contacts immediately adjacent to old ones, then the net effect is to decrease the average age of contacts overall. As shearing continues, the subsequent evolution of state and friction may be described by either the Dieterich or Ruina evolution laws.

We fit both the Dieterich and Ruina laws to the normal stress step simulations through forward modeling by solving (2), (3), and (6) using either (4) or (5) as the evolution law. A fifth-order Runga-Kutta method was used and our modeling included the measured effects of Poisson expansion for our apparatus ($\Delta\tau/\Delta\sigma_n$), determined to be 0.01 for the Westerly testing blocks and 0.02 for steel testing blocks. We found appropriate parameters for a, b, and D_c from a least squares iterative inversion of velocity steps performed during the same experiment as the normal stress steps. We found that in general, $\alpha = 0.3$ (Figure 7) did not fit the data well, as the Dieterich model overshoots the the final steady state sliding stress and the Ruina model does not match the slope of the data during elastic shear loading (Figure 16a). Using $\alpha = 0.2$ provided a better fit (Figure 16b). The Ruina model matches the data quite well, especially on the initial shear loading, but the Dieterich

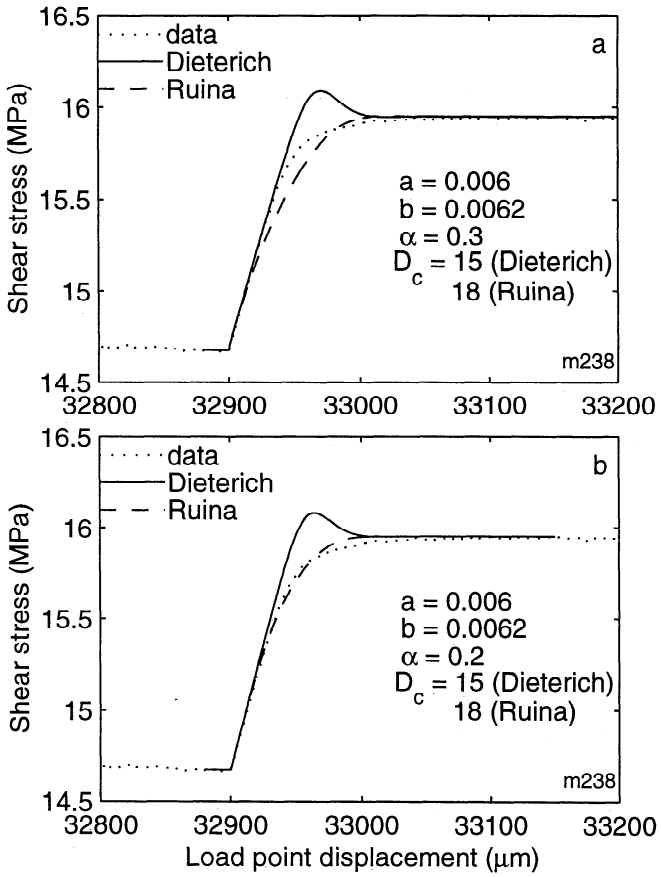

Figure 16. Shear stress (MPa) versus shear load point displacement (μm) for one normal stress step of 8.8% of the initial normal stress. The frictional parameters used here were $a = 0.006, b = 0.0062, D_c = 18$ μm (Ruina), $D_c = 15$ μm (Dieterich), (a) $\alpha = 0.3$ and (b) $\alpha = 0.2$. The parameters a, b, and D_c were obtained from modeling a velocity step from this same experiment.

model still overshoots the final steady state shear stress. None of our data show such overshoots. For the range of friction parameters that we considered "reasonable" based on fits to velocity steps in the same experiments (e.g., velocity weakening), we found that the Dieterich model consistently overshot the final steady state shear stress. Even though the Dieterich model does not fit the data well in general, since the Ruina law does a good job when $\alpha = 0.2$, this is the value of α we used in the simulations of vibrational slide-hold-slide tests discussed next.

4.3. Normal Stress Oscillations

Harmonic oscillations of the normal stress during quasi-stationary contact increases the absolute level of frictional healing by an amount that is roughly proportional to the amplitude of oscillations. This result can be approximately compared to the results of the normal stress "pulse tests" of *Linker and Dieterich* [1992], who found that a sudden very short (0.2-s) increase in normal stress during a 1-s hold was followed by a peak in friction that was larger than peak friction for holds of similar duration without a normal stress pulse. Likewise, they found that the absolute level of peak friction increased as the magnitude of the stress pulses increased. Their experiments were carried out in double direct shear as well, but with sample sizes of 5 × 5 cm and a mean normal stress of only 5 MPa. The similarity between our results and theirs suggests that our results are valid for at least this range of laboratory scales.

We modeled vibrational slide-hold-slide data with two goals in mind. We tried to fit data from single holds with forward models using parameters derived from modeling velocity steps, and we also tried to use similar parameters to model the frictional healing trends. We added normal stress vibrations to the simulations by specifying a 1-Hz sine wave as the normal stress during the hold. In order to match the experimental time series of a given slide-hold-slide test, we lagged the start of the normal stress vibrations in relation to the beginning of the hold. This lag corresponded to t_1-t_2 in Figure 9, for example. We also ramped the normal stress sine wave amplitude in the simulation up to the final vibrational amplitude linearly over the same ramp time as was done manually during the experiments (t_2-t_3 in Figure 9). In experiments we ramped down normal stress at the end of the hold in order to maintain constant vibration frequency and to avoid sudden, uncontrolled changes in normal stress associated with jumping back to our nominal normal stress. In the simulations we ended the hold at a zero crossing of the sine wave.

Figure 17 shows data and models for one hold from the experiment in Figure 8. In this example, initial lag time was 1 s, and the initial ramp was 5 s long. The simulated normal stress matches the experimental values well, except for a slight DC level offset resulting from the added experimental signal not being perfectly symmetric around the mean normal stress (Figure 17b). The simulations of shear stress during and after a hold with vibrations shown in Figure 17a are examples of typical results of forward models that used friction parameters derived from modeling earlier velocity steps and constant stress slide-hold-slide tests. The Dieterich evolution law (shaded line) fits the data well during the hold but gives a peak shear stress that is too large and a subsequent return to steady state that is too fast. We could not simultaneously fit relaxation during the hold and peak stress after the hold for any reasonable range of parameters ($0.006 \leq a \leq 0.015, -0.002 \leq (a-b) \leq 0.002$, 5 μm $\leq D_c \leq$ 30 μm). In all cases the Dieterich law gave a sharp peak friction, which we did not observe in the data.

The Ruina law (dotted line) does not fit the relaxation time series data very well because of an early stress drop. We often observed similar stress drops in the experiments for large-amplitude holds (Figure 12), but models using the Ruina law and reasonable friction parameters consistently resulted in stress drops that were larger than observed. To suppress these large

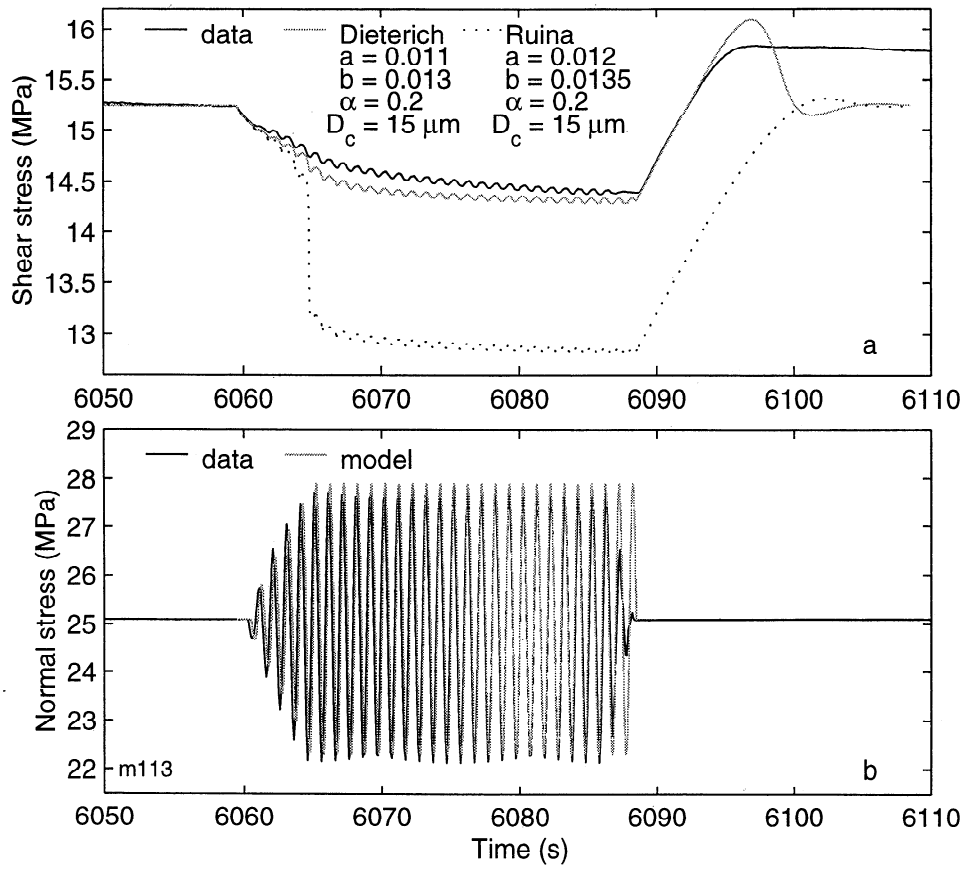

Figure 17. (a) Shear stress and (b) normal stress as a function of time for one 30-s hold from the experiment shown in Figure 8. The solid line shows data, the shaded line shows the model using the Dieterich evolution law, and the dotted line shows the model using the Ruina evolution law. Figure 17b shows only one model line since we used the same normal stress time series for both simulations.

stress drops, D_c had to be $\sim$ 200 μm, over an order of magnitude larger than we expected based on models of velocity steps or slide-hold-slide tests at constant stress. At the end of the hold the Ruina model has a more rounded peak in friction, which is encouragingly similar to experimental observations but, like the Dieterich model, returns to steady state friction faster than observed in the data. When velocity strengthening conditions were specified ($a-b>0$), the Ruina model exhibited a value and shape of peak friction that was similar to what we found experimentally, but we could never reproduce the delayed return to steady state. The slow return to steady state observed experimentally and large effective D_c are probably due to gouge layer effects such as reformation of vibrationally disrupted shear bands, which cannot be accommodated by the present constitutive laws (N.H. Sleep et al., Physics of friction and strain rate localization in simulated fault gouge, submitted to *Journal of Geophysical Research*, 1999).

Though the rate- and state-variable formulation that we use does not reproduce time series data of individual holds well (Figure 17), it is still important to test whether macroscopic behaviors of the system, such as healing and relaxation rates, are described well. If so, we can conclude that this formulation approaches the correct solution. Therefore we used forward models of both evolution laws and the same friction parameters used in Figure 17 to fit healing curves from an experiment with 11.5-MPa vibrations (Figure 18). We used a single set of friction parameters for each law and modeled sets of slide-hold-slide tests both at constant stress and with 11.5-MPa double amplitude over the range in hold times of 3-1000 s. The simulation that used the Ruina law does a good job of fitting both the absolute level of total shear stress change as well as the small rate of change with hold time. For the range of reasonable values of a and b that we explored ($0.007 \leq a \leq 0.00135, a-b<0$), the results of the Ruina model were basically unchanged from the example shown here. Most changes in a and b affect healing and relaxation oppositely; thus adding the two measurements negates these changes. Increasing or decreasing D_c lowered or raised the DC level of the healing curve, respectively. Thus the parameters that we chose based on typical fits to other friction data also give the best global fit to healing data when the Ruina evolution model is used (Figure 18).

In contrast, the Dieterich simulation grows too large

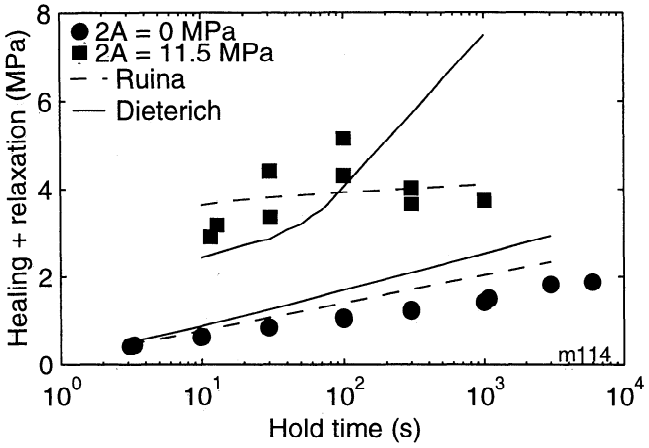

Figure 18. Data (solid symbols) and models using the Dieterich (solid line) and Ruina (dashed line) laws of healing plus relaxation as a function of hold time for two sets of slide-hold-slide tests from one experiment. Circles show data without vibrations and squares show data with 11.5-MPa vibrations during the holds. Parameters are the same as in Figure 17.

too fast so that it does not describe the overall behavior of the system well for hold times > 100 s. Exploration of parameter space led to similar results as with the Ruina law in that changes in a and b were negligible and changes in D_c changed the absolute values of the curve but not its slope. Our data consistently showed a nearly flat healing curve as predicted by the Ruina law.

In addition, we fit the data in Figure 11d with both laws and the same parameter values as in Figure 17 (Figure 19). Both laws are able to reproduce the trend of increasing total frictional strength with increasing amplitude of vibration. Therefore both evolution laws can recover the DC level change in frictional strength that occurs when vibration amplitude is increased for $t_h \leq 100$ s. The Dieterich law does not fit observations at $t_h > 100$ s.

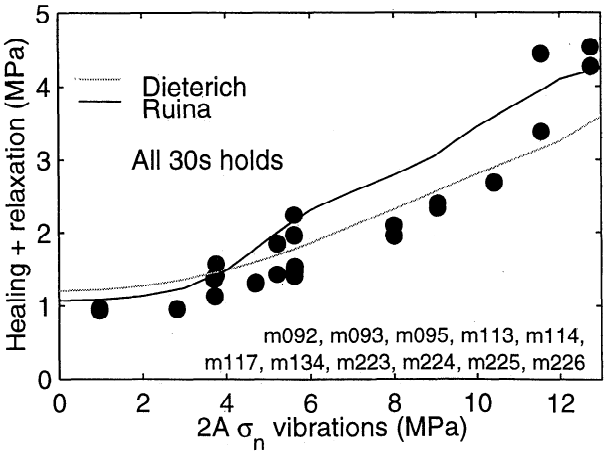

Figure 19. Data (solid symbols) and models (lines) of healing plus relaxation as a function of $2A$ for 30-s hold times. Parameters are the same as in Figure 17.

4.4. Micromechanical Interpretation

A major shortcoming in the present formulations of the friction constitutive laws is that they do not account for the gouge layer effects which are likely to be extremely important in characterizing the behavior of the system. Mechanical consolidation of gouge has been shown to play a role in the frictional strengthening process [*Nakatani*, 1998]. It is clear from our data of both normal stress steps (Figure 6) and holds with vibrations (Figures 10 and 13) that porosity decreases dramatically in response to an applied external normal

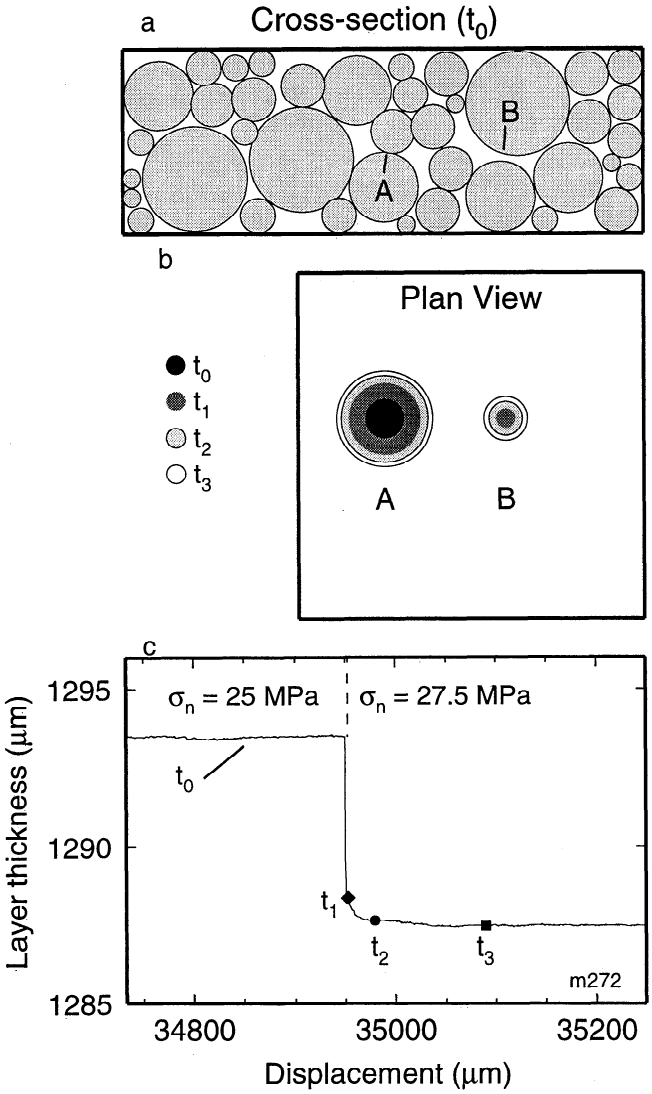

Figure 20. Contact junction evolution in a granular medium in response to a sudden increase in normal stress. (a,b) Sketches of the granular assemblage in cross section and of hypothetical contact junctions in plan view. (c) Figure 6c is shown for reference. Initially, the system is shearing in steady state with some assemblage of grain sizes and junctions (Figure 20a and section marked t_0 in Figure 20c). Contact A exists, but B does not yet. The normal stress step compacts the layer causing growth of A and producing contact B (t_1). The elastic shear load up (t_2) and evolution to a new steady state (t_3) cause growth of the two contacts.

stress. In the case of the normal stress steps it is somewhat straightforward to consider that a sudden increase in normal stress compresses the granular material elastically, then shearing continues to compact the grains faster since the pressure is now greater (Figure 20). After further shearing, the porosity of the granular assemblage reaches a new steady state that is lower than the previous porosity. Grain contacts become more numerous and larger than at the previous lower normal stress (Figure 20).

The behavior of granular layers under normal stress vibrations is probably more complicated. For the displacements of our slide-hold-slide tests (≈10-35 mm), we had reached a steady value of sliding friction and were in the regime characterized by localized shear along Riedel, B, and Y shear bands [*Mair and Marone*, 1999]. In a slide-hold-slide test at constant normal stress we envisage that frictional strengthening occurs throughout the layer as contacts grow and strengthen, then are disturbed as slip is reinitiated, causing the observed peak in friction after the hold. In order to account for the greater degree of both relaxation and compaction that we have observed for vibrational slide-hold-slide tests the external oscillations must physically promote the strengthening of shear bands and regions external to shear bands (N.H. Sleep et al., Physics of friction and strain rate localization in simulated fault gouge, submitted to *Journal of Geophysical Research*, 1999). If the normal stress were simply increased in a one-sided step during holds, then the shear band restrengthening would be faster solely as a result of the greater pressure. Instead, when normal stress is vibrated, gouge particles become compacted into a lower energy configuration. Our interpretation is that this disrupts the shear band's porosity, width, and boundary configuration. Effectively, we expect that vibrations widen the zone of gouge particles involved in active shearing, thus increasing the barrier to sliding to a greater degree than by mere contact junction growth. This mechanism may also explain the rounded peaks in friction observed on the reload (Figure 8). If the shear bands have been disrupted enough, overcoming frictional resistance may occur at slightly different times along parts of the shear band as it reforms, making the overall peak not as clearly evident and increasing the time or displacement to return to steady state.

Without microstructural observations of gouge layers to confirm our hypotheses, it is difficult to conclude exactly what mechanism is responsible for the increased frictional strengthening during vibrational holds. Nevertheless, monitoring changes in porosity of the gouge layer under external stressing is important for determining how to add these effects to the present frictional constitutive laws.

4.5. Relevance to Tectonic Faults

The observation that the return to steady state friction was delayed after attaining a peak value of friction following a vibrational hold (Figure 8) is consistent with an increase during vibration of the critical slip distance (D_c), which is the characteristic distance over which dynamic rupture is initiated on a fault [*Marone and Kilgore*, 1993]. Furthermore, observations of repeating earthquakes on faults suggest that earthquake stress drops increase with increasing recurrence interval between earthquakes by a factor that is larger than the value obtained from direct extrapolation from laboratory measurements of frictional healing [*Vidale et al.*, 1994; *Marone et al.*, 1995; *Marone*, 1998a]. Our results imply that typical laboratory frictional healing experiments at room conditions are measuring a minimum value of restrengthening since they assume that all applied tectonic loads are constant during quiescent intervals; these results are consistent with work on the effect of shear load on healing [*Karner and Marone*, 1998]. (However, our results do not provide information for other conditions, such as low humidity, [e.g., *Frye and Marone*, 1999]).

Nearby faults are likely to interact with one another, as coseismic changes in creep velocities on parts of the San Andreas fault due to nearby moderate earthquakes have shown [*King et al.*, 1977; *Mavko*, 1982]. Our results predict that a transient dynamic normal load during creep can strengthen a fault, a result also predicted from a numerical analysis by *Mavko* [1982] in which a series of earthquakes on the Busch fault in southern California caused decreased slip rates and possibly locking on the adjacent Calaveras fault. Since the Busch fault is nearly perpendicular to the Calaveras fault, most of the stress from the Busch earthquakes would have been resolved onto the Calaveras fault in the normal direction, similar to our laboratory experiment.

We did not attempt to scale the amplitudes and frequencies of normal force variations in our experiments to any particular tectonic system. We also did not test the effects of a range of frequencies or changes in frequency, nor did we test the effects of transient shear stresses [e.g., *Gomberg et al.*, 1998] on frictional healing. Nevertheless, our results can be interpreted in light of such processes as the rate and degree of fault restrengthening and nucleation patch size growth during repeating earthquake cycles. Experiments such as those we have conducted can be valuable for characterizing the effect of transient stresses on creeping faults.

5. Conclusions

We have observed and compared frictional healing and relaxation for slide-hold-slide tests at constant stress for ranges of displacements and found that an increase in the parameter b in the rate and state friction laws adequately accounts for the increase in healing and simultaneous decrease in relaxation that we observe with displacement. We examined the effects of external stressing on fault friction by conducting both normal stress step tests at constant velocity and normal stress vibration tests during quasistationary contact. Our observations of normal stress steps show that

following a step change in normal stress, shear stress increases elastically, then evolves to a new steady state, confirming the results of *Linker and Dieterich* [1992]. We also observed an elastic decrease in the porosity of the gouge layer followed by further evolution in the same direction until a new steady state compaction rate was reached. The Ruina law, in general, provided a better fit to the normal stress step data than the Dieterich law. Our observations of normal stress vibrations during slide-hold-slide tests show that frictional relaxation and subsequent healing are both greatly enhanced by vibrations; this enhancement is greater for larger-amplitude vibrations. Modeling the global characteristics of frictional healing as a function of hold time and vibration amplitude were successful at small hold times for the Dieterich law and, in general, for all the ranges of hold times and amplitudes that we tested experimentally for the Ruina law. However, we were unable to reproduce adequately the observed time series data of any given hold with vibrations using either law. We believe that the discrepancies between the observed behavior and that predicted by the present formulation of the friction constitutive laws are due to neglecting the important effects of changing gouge layer porosity and alteration of the shear bands during external normal stressing. Future work will need to focus on this aspect of understanding the effects of applied stresses if we hope to relate experimental data and simulations to tectonic situations.

Acknowledgments. The authors thank reviewers Terry Tullis, Frederick Chester, and the Associate Editor for suggestions that helped to clarify the presentation. Discussions with Norm Sleep refined our interpretations of the data. We also thank Steve Karner, Karen Mair, and Kevin Frye for lending us their considerable experimental expertise.

References

Beeler, N. M., T. E. Tullis, and J. D. Weeks, The roles of time and displacement in the evolution effect in rock friction, *Geophys. Res. Lett.*, *21*, 1987–1990, 1994.

Beeler, N. M., T. E. Tullis, M. L. Blanpied, and J. D. Weeks, Frictional behavior of large displacement experimental faults, *J. Geophys. Res.*, *101*, 8697–8715, 1996.

Bronicc, Z., and W. Lenkiewicz, Static friction processes under dynamic loads and vibration, *Wear*, *80*, 261–271, 1982.

Delour, J., A. Kudrolli, and J. P. Gollub, Velocity statistics in excited granular media, *Chaos*, *9*, 682–690, 1999.

Dieterich, J. H., and M. F. Linker, Fault stability under conditions of variable normal stress, *Geophys. Res. Lett.*, *19*, 1691–1694, 1992.

Dieterich, J. H., Time-dependent friction in rocks, *J. Geophys. Res.*, *77*, 3690–3697, 1972.

Dieterich, J. H., Time-dependent friction and the mechanics of stick-slip, *Pure Appl. Geophys.*, *116*, 790–805, 1978.

Dieterich, J. H., Modeling of rock friction, 1, Experimental results and constitutive equations, *J. Geophys. Res.*, *84*, 2161–2168, 1979.

Dieterich, J. H., Constitutive properties of faults with simulated gouge, in *Mechanical Behavior of Crustal Rocks, Geophys. Monogr. Ser.*, edited by N. L. Carter et al., vol. 24, pp. 103–120, AGU, Washington, D.C., 1981.

Dieterich, J. H., Probability of earthquake recurrence with nonuniform stress rates and time-dependent failure, *Pure and Appl. Geophys.*, *126*, 589–617, 1988.

Frye, K. M., and C. Marone, Humidity dependence of healing and frictional creep in simulated fault gouge (abstract), *EOS Trans. AGU*, *80*, S329, 1999.

Gomberg, J., M. L. Blanpied, and N. M. Beeler, Transient triggering of near and distant earthquakes, *Bull. Seismol. Soc. Am.*, *87*, 294–309, 1997.

Gomberg, J., N. M. Beeler, M. L. Blanpied, and P. Bodin, Earthquake triggering by transient and static deformation, *J. Geophys. Res.*, *103*, 24,411–24,426, 1998.

Hess, D., and A. Soom, Normal vibrations and friction under harmonic loads, part I, Hertzian contacts, *J. Tribol.*, *113*, 80–86, 1991.

Hill, D., et al., Seismicity remotely triggered by the magnitude 7.3 Landers, California, earthquake, *Science*, *260*, 1617–1623, 1993.

Johnson, T., Time-dependent friction of granite: Implications for precursory slip on faults, *J. Geophys. Res.*, *86*, 6017–6028, 1981.

Karner, S. L., and C. Marone, The effect of shear load on frictional healing in simulated fault gouge, *Geophys. Res. Lett.*, *25*, 4561–4564, 1998.

King, C. Y., R. D. Nason, and R. O. Burford, Coseismic steps recorded on creepmeters along the San Andreas fault, *J. Geophys. Res.*, *82*, 1655–1661, 1977.

Kudrolli, A., M. Wolpert, and J. P. Gollub, Cluster formation due to collisions in granular material, *Phys. Rev. Lett.*, *78*, 1383–1386, 1997.

Linker, M., and J. H. Dieterich, Effects of variable normal stress on rock friction: Observations and constitutive equations, *J. Geophys. Res.*, *97*, 4923–4940, 1992.

Lockner, D., R. Summers, and J. Byerlee, Effects of temperature and sliding rate on frictional strength of granite, *Pure Appl. Geophys.*, *124*, 445–469, 1986.

Mair, K., and C. Marone, Friction of simulated fault gouge for a wide range of velocities, *J. Geophys. Res.*, in press, 1999.

Marone, C., Laboratory-derived friction laws and their application to seismic faulting, *Annu. Rev. Earth Planet. Sci.*, *26*, 643–696, 1998a.

Marone, C., The effect of loading rate on static friction and the rate of fault healing during the earthquake cycle, *Nature*, *391*, 69–72, 1998b.

Marone, C., and B. Kilgore, Scaling of the critical slip distance for seismic faulting with shear strain in fault zones, *Nature*, *362*, 618–621, 1993.

Marone, C., C. B. Raleigh, and C. H. Scholz, Frictional behavior and constitutive modeling of simulated fault gouge, *J. Geophys. Res.*, *95*, 7007–7025, 1990.

Marone, C., J. E. Vidale, and W. L. Ellsworth, Fault healing inferred from time dependent variations in source properties of repeating earthquakes, *Geophys. Res. Lett.*, *22*, 3095–3098, 1995.

Mavko, G. M., Fault interaction near Hollister, California, *J. Geophys. Res.*, *87*, 7807–7816, 1982.

Mavko, G. M., S. Schulz, and B. D. Brown, Effects of the 1983 Coalinga, California, earthquake on creep along the San Andreas fault, *Bull. Seismol. Soc. Am.*, *75*, 475–489, 1985.

Nakatani, M., A new mechanism of slip weakening and strength recovery of friction associated with the mechanical consolidation of gouge, *J. Geophys. Res.*, *103*, 27,239–27,256, 1998.

Polycarpou, A. A., and A. Soom, Boundary and mixed friction in the presence of dynamic normal loads, part I, System model, *J. Tribol.*, *117*, 255–260, 1995a.

Polycarpou, A. A., and A. Soom, Boundary and mixed fric-

tion in the presence of dynamic normal loads, part II, Friction transients, *J. Tribol.*, *117*, 261–266, 1995b.

Rice, J. R., and J.-C. Gu, Earthquake aftereffects and triggered seismic phenomena, *Pure Appl. Geophys.*, *121*, 187–219, 1983.

Ruina, A., Slip instability and state variable friction laws, *J. Geophys. Res.*, *88*, 10,359–10,370, 1983.

Scott, D. R., C. J. Marone, and C. G. Sammis, The apparent friction of granular fault gouge in sheared layers, *J. Geophys. Res.*, *99*, 7231–7246, 1994.

Skåre, T., and J.-E. Ståhl, Static and dynamic friction processes under the influence of external vibrations, *Wear*, *154*, 177–192, 1992.

Spudich, P., L. K. Steck, M. Hellweg, J. B. Fletcher, and L. M. Baker, Transient stresses at Parkfield, California, produced by the *M* 7.4 Landers earthquake of June 28, 1992: Observations from the UPSAR dense seismograph array, *J. Geophys. Res.*, *100*, 675–690, 1995.

Tullis, T. E., and J. D. Weeks, Constitutive behavior and stability of frictional sliding of granite, *Pure Appl. Geophys.*, *124*, 383–414, 1986.

Tworzydlo, W. W., and E. Becker, Influence of forced vibrations on the static coefficient of friction–Numerical modeling, *Wear*, *143*, 175–196, 1991.

Vidale, J. E., W. L. Ellsworth, A. Cole, and C. Marone, Variations in rupture process with recurrence interval in a repeated small earthquake, *Nature*, *368*, 624–626, 1994.

Wang, C., and Y. Cai, Sensitivity of earthquake cycles on the San Andreas fault to small changes in regional compression, *Nature*, *388*, 158–161, 1997.

Wang, W., and C. H. Scholz, Micromechanics of the velocity and normal stress dependence of rock friction, *Pure and Appl. Geophys.*, *143*, 303–315, 1994.

C. Marone and E. Richardson, Department of Earth Atmospheric and Planetary Sciences Massachusetts Institute of Technology, Cambridge, MA 02139. (cjm@westerly.mit.edu; eliza@mit.edu)

(Received December 10, 1998; revised July 8, 1999; accepted September 7, 1999.)